USGS
science for a changing world

Prepared in Cooperation with the U.S. Army Corps of Engineers

Measurement of Near-Surface Seismic Compressional Wave Velocities Using Refraction Tomography at a Proposed Construction Site on the Presidio of Monterey, California

By Michael H. Powers and Bethany L. Burton

Open-File Report 2012–1191

U.S. Department of the Interior
U.S. Geological Survey

U.S. Department of the Interior
KEN SALAZAR, Secretary

U.S. Geological Survey
Marcia McNutt, Director

U.S. Geological Survey, Reston, Virginia, 2012

For product and ordering information:
World Wide Web: http://www.usgs.gov/pubprod
Telephone: 1-888-ASK-USGS

For more information on the USGS—the Federal source for science about the Earth,
its natural and living resources, natural hazards, and the environment:
World Wide Web: http://www.usgs.gov
Telephone: 1-888-ASK-USGS

Suggested citation:
Powers, M.H., and Burton, B.L., 2012, Measurement of near-surface seismic compressional wave velocities using refraction tomography at a proposed construction site on the Presidio of Monterey, California: U.S. Geological Survey Open-File Report 2012–1191, 17 p.

Prepared under Interagency Agreement Number W62N6M03094140.

Contents

Abstract 1
Introduction 1
Geological Background 1
Seismic Refraction Method 3
Seismic Refraction Survey 4
  Data Acquisition 4
  Data Processing and Inversion 7
  Inversion Results 7
Conclusions 13
Acknowledgments 13
References Cited 13
Appendix 1: Seismic Refraction Traveltime Curves 14

Figures

1. Survey site location map with the Monterey peninsula geologic map underlaid 2

2. Aerial photograph showing the locations of the two seismic lines 5

3. Photos of seismic equipment deployed on Line A 6

4. Photos of seismic equipment deployed on Line B 6

5. A) P-wave velocity versus lateral and vertical position under Line A is shown in profile view. B) An interpretation of general material types is shown based on velocity 8

6. A) P-wave velocity versus lateral and vertical position under Line B is shown in profile view. B) An interpretation of general material types is shown based on velocity 9

7. Rippability chart for the smallest Caterpillar machine 11

8. Map showing the locations of previously mapped Quaternary faults on the Monterey peninsula 12

Conversion Factors

Inch/Pound to SI

Multiply	By	To obtain
	Length	
foot (ft)	0.3048	meter (m)
mile (mi)	1.609	kilometer (km)
	Mass	
pound, avoirdupois (lb)	0.4536	kilogram (kg)

Vertical coordinate information is referenced to the National Geodetic Vertical Datum of 1929 (NGVD 29).
Horizontal coordinate information is referenced to the North American Datum of 1983 California State Plane zone 4 (CS83 zone 4).
Depth below ground surface, as used in this report, refers to distance below the vertical datum.

Measurement of Near-Surface Seismic Compressional Wave Velocities Using Refraction Tomography at a Proposed Construction Site on the Presidio of Monterey, California

By Michael H. Powers and Bethany L. Burton

Abstract

The U.S. Army Corps of Engineers is determining the feasibility of constructing a new barracks building on the U.S. Army Presidio of Monterey in Monterey, California. Due to the presence of an endangered orchid in the proposed area, invasive techniques such as exploratory drill holes are prohibited. To aid in determining the feasibility, budget, and design of this building, a compressional-wave seismic refraction survey was proposed by the U.S. Geological Survey as an alternative means of investigating the depth to competent bedrock. Two sub-parallel profiles were acquired along an existing foot path and a fence line to minimize impacts on the endangered flora. The compressional-wave seismic refraction tomography data for both profiles indicate that no competent rock classified as non-rippable or marginally rippable exists within the top 30 feet beneath the ground surface.

Introduction

A new barracks structure is being planned for construction on the Presidio of Monterey, located in Monterey, Calif., in woodlands between existing barracks and the Post Exchange (PX). Planning for excavation of the barracks foundation requires knowledge of the depth to what may be shallow granodioritic bedrock. However, permits have not been issued for invasive access with drill rigs that will harm the endangered flora present in the area: an orchid (piperia yadonii) that lies dormant for much of the year as a fragile tuber in the soft forest floor materials. To determine depth to bedrock and progress with the construction-planning procedures, the U.S. Geological Survey (USGS) designed, acquired (using a handheld hammer source), and analyzed two seismic refraction profiles. This report presents the results of the seismic-profile surveys across the existing woodlands. Because the U.S. Army Corps prefers that English units (also called Imperial units or foot-mile-pound units) are used instead of SI units, distances and weights were recorded in and are reported here in English units.

Geological Background

A geologic map (fig. 1) by Clark and others (1997) shows the site location within Cretaceous-age (145 to 65 million years ago (Ma)) porphyritic granodiorite (unit Kgdp on the map). Pleistocene (2.6 Ma to 11.7 thousand years ago (ka)) marine coastal terrace deposits (units Qctm and Qcth) are present above and below the granodiorite outcrops.

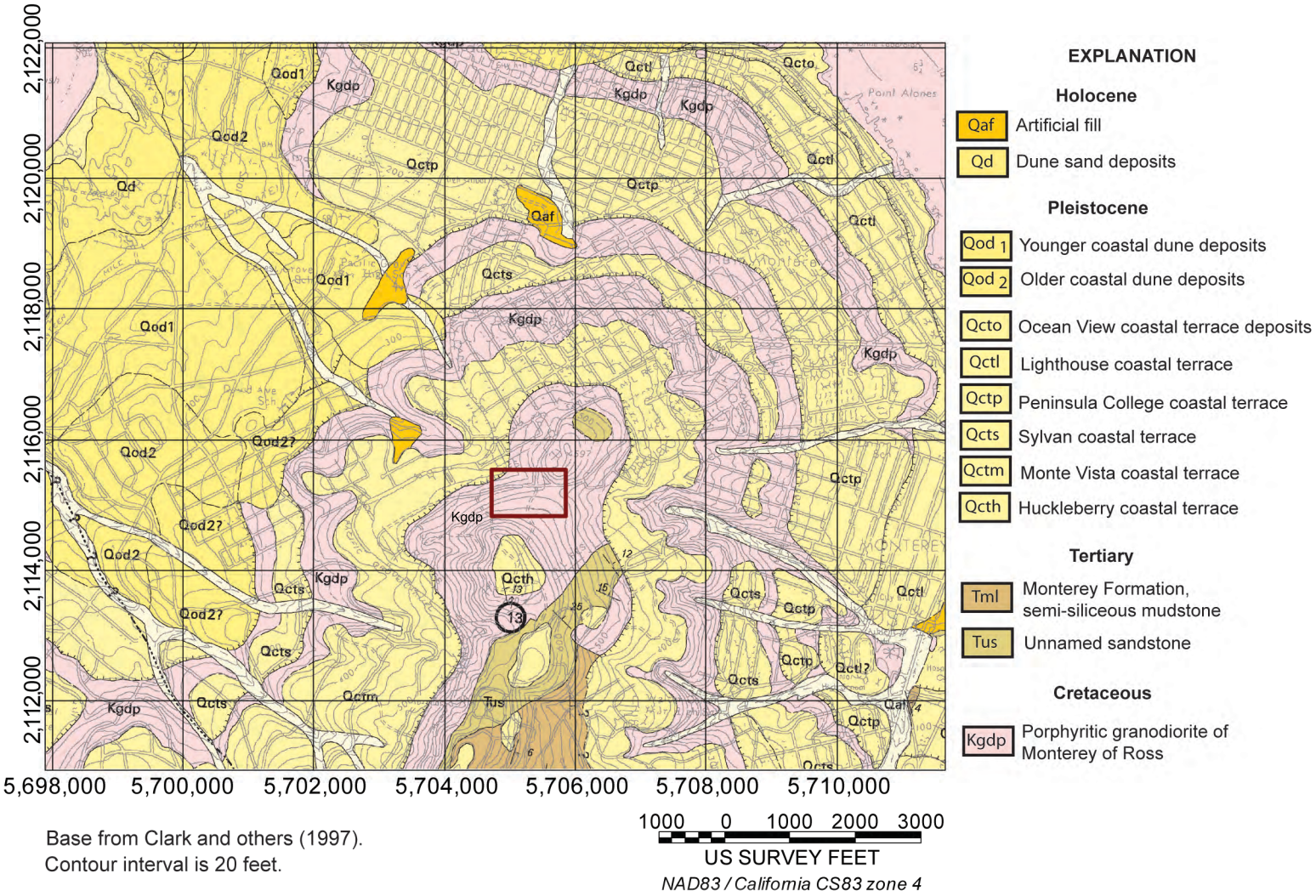

Figure 1. Survey site location map with the Monterey peninsula geologic map (Clark and others (1997)) underlaid. Red rectangle indicates survey area shown in figure 2.

Immediately south of the site, an unnamed marine, arkosic sandstone (unit Tus), derived principally from granitic rocks and deposited around 15 Ma, is present.

Because the proposed construction site is covered with a layer of soil of unknown thickness with no outcrops, analysis of the geologic map and nearby observations led to speculation about the depth to competent bedrock. A large outcrop immediately east of the site on the Presidio property was exposed during recent construction and shows a transition of marine coastal terrace deposits into weathered and increasingly more competent granodiorite bedrock. Construction planning requires knowledge of the rippability of the subsurface materials that will be encountered during foundation excavation, so depth to competent bedrock is an important factor.

Rippability is a qualitative property of rock; it describes the relative ease with which the material can be removed using excavation equipment. There are three classifications: rippable (easily removed), marginal, and non-rippable (difficult to remove). Rippability classification is more reliably correlated with seismic compressional-wave (P-wave) velocities than with geological rock type (Bailey, 1975; MacGregor and others, 1994). For example, weathered granite may exhibit a slower P-wave velocity than competent sandstone, and in such a case, the weathered granite will be more easily excavated than the competent sandstone. In this regard, and for this survey, the measure of P-wave velocity laterally and with depth across the proposed construction site is of more interest than the classification type of the geological materials. The requested maximum depth of investigation based on the estimated foundation depth of the proposed buildings was approximately 30 feet (ft).

Seismic Refraction Method

The seismic-profiling method makes use of a seismic source and a linear array of geophones spaced at regular intervals across the ground surface (Beck, 1981; Reynolds, 1997; Sharma, 1997). When a geophone is well-coupled to the earth (usually with a spike), it generates an output voltage that is proportional to the vibrational motion of the ground in response to the seismic source and other vibrational sources. Modern geophones are sensitive enough that, in the absence of other noise, footsteps within 50- to 100-ft can be detected easily. A central acquisition unit simultaneously records the output of each of the geophones for an established amount of time and with a selected sampling frequency. The acquisition is started by a trigger, usually coordinated with the impact of the seismic source on the ground.

The seismic source can be a person striking the ground with a sledgehammer, a truck-mounted and truck-powered heavy hammer impact, a controlled vibration, a gunshot into the ground, a buried explosive charge, or any other method to generate ground vibrations. A good source has the following properties: (1) its waveform signature recorded by the geophones must be recognizable, (2) its strength must be adequate for the project goals, (3) it must be transportable, repeatable, and cost-efficient, and (4) it must be able to consistently and accurately trigger the system. For this project, we used a handheld 12-pound sledgehammer hitting a carefully placed steel plate for portability and to avoid damage to endangered flora.

When the source imparts energy into the ground and the trigger system initiates measurement of all geophone responses (starting at the instant of impact), the recorded response of the geophones is called a “shot record.” The shot record displays ground-

motion variations with traveltime (y-axis) and distance (x-axis). With basic understandings of the physics of seismic-wave propagation through the earth and through the local geology, arrival events are recognizable on the shot record. Such events include the initial direct compressional wave energy radiating outward from the source as well as head-wave energy, which enters and leaves relatively higher-velocity layers at a critical angle dependent on the velocity contrast. The seismic refraction method uses the first-arrival traveltimes of the direct and head waves to gain understanding of subsurface velocity variations. Other arrival events such as reflected-wave energy, surface-wave energy, and air-wave energy are present on the shot record but not used by the refraction method.

Seismic Refraction Survey

Data Acquisition

The USGS acquired two generally east-west trending seismic lines (fig. 2). Line A is the northern profile and is located approximately along the pedestrian pathway through the woodlands (fig. 3). The topography is lowest on the west end and climbs gradually, becoming steeper on the east end. Total topographic relief across the line is about 45 ft. The southern profile, Line B, is located uphill and south of the pedestrian pathway along the north side of the fence line that separates the woodlands of the City of Monterey Huckleberry Hill Nature Preserve from the Presidio (fig. 4). Much of Line B is located at about 550 ft elevation, with an approximately 20-ft deep valley near the middle of the line. The ground along Line B was thick, soft, spongy forest-floor material that was not good for geophone coupling or for hammer source energy propagation. As a result, the first-arrival time picks for Line B are constrained to more limited source-receiver offset distances than are achieved along Line A.

The number of live channels multiplied by the spacing between live geophones (one live geophone per live channel) determines the maximum source-receiver offset, assuming source locations are within the geophone spread. For design purposes, we conservatively estimate the maximum depth of investigation for the seismic refraction method to be about one-fifth of the maximum source-receiver offset. The presence of traffic noise at the site could decrease the signal-to-noise ratio at the far offsets and limit the depth of investigation. The acquisition geometry was designed based on a target maximum depth of investigation of approximately 100 ft. In practice, the limited-strength hammer blows in the soft soil and the site noise restricted our first-arrival traveltime picks to source-receiver offsets of between 200 and 300 ft. However, the high velocity of the bedrock material at depth still allowed velocity imaging to a maximum depth of approximately 100 ft.

Both lines were acquired with a single, fixed spread of 96 40-Hertz compressional-wave geophones spaced 6 ft apart (downline positions 6, 12, 18, … , 576 ft). Source stations were located every 24 ft between and in-line with receivers starting at one-half station before the first geophone (downline positions 3, 27, 51, … , 579 ft). For both profiles and for each source station, four blows with the sledgehammer were recorded and saved independently. The shot records were then reviewed, and the best record for each station was selected for picking first-arrival traveltimes on each trace.

Figure 2. Aerial photograph of the survey site indicating the locations of seismic lines A and B, shown in blue. The extents of the low velocity zone at depth shown in figures 5 and 6 are shown as yellow rectangles on each of the lines.

Figure 3. Photos of the seismic equipment deployed on Line A along the footpath looking *A*, west and *B*, east.

Figure 4. Photos of the seismic equipment deployed on Line B looking *A*, southwest and *B*, east-northeast.

The source and receiver stations were located with a tape and surveyed with a handheld Garmin etrex Vista HCx global positioning system (GPS) unit (Garmin International, Olathe, Kans.). This unit uses satellite positioning for latitude, longitude, and for approximate elevation. It refines local elevation changes with a barometric pressure-based altimeter. Accuracy for all measurements is only good to within 2–5 meters for this instrument. We improved this accuracy by acquiring full x, y, and z position data every 1 second while making multiple slow passes across each line. The resulting overlapping data points were mathematically fit for an approximate position and elevation across each profile. The relative elevation results were confirmed and then adjusted based on a 5-ft contour map provided by the project engineers and also based on detailed line descriptions of elevation changes recorded in the field.

Data Processing and Inversion

The shot records were frequency-filtered using a band-pass filter to remove undesirable data that can mask the desired source signal. Although the band-pass filter aids in the picking process by removing unwanted noise, it also leads to artificially early first-arrival traveltimes. It is therefore imperative to pick the first breaks (the first arrival of direct and head wave energy for the various layers) by comparing both the filtered and unfiltered data and identifying the location within the first-arrival wavelet in the filtered data that corresponds to the true first-arrival traveltime in the unfiltered data. The resultant traveltime picks were displayed as curves representing the first-arrival time versus source-receiver lateral position across the line of active geophones. The traveltime curves are presented in Appendix 1.

The measured first-arrival traveltime data are combined with the surveyed positions and elevations and are input into the inversion algorithm Rayfract (Intelligent Resources, Inc., Canada). For this study, a starting velocity model with the correct source and receiver geometry was generated from one-dimensional velocity soundings based on the first-arrival traveltime data for each common midpoint. A common midpoint is a group of source-receiver pairs that have a common surface location that corresponds with the center location between those pairs. With this starting model and the measured data, the Rayfract algorithm performs an inversion following the wavepath eikonal traveltime (WET) method (Schuster and Quintus-Bosz, 1993), using the maximum-smoothing option applied during the inversion.

In the inversion process after the first comparison of traveltime differences (between measured and calculated traveltimes), the model is updated and new calculated traveltime curves are created and compared to the data. This procedure continues for a fixed number of iterations until convergence is reached on a “best-fit” solution. Generally, a smooth solution with an approximate fit is regarded as more geologically realistic than a very rough solution with an exact fit, because the rough solution may be adding unnecessary structure to fit noise in the data. In practice, noisier data require more smoothing and have an overall lower fit accuracy.

Inversion Results

Figures 5 and 6 show our final solutions for Lines A and B, respectively, after ten iterations each. The root-mean-square (RMS) error for Line A is 1.74 milliseconds (ms) with a corresponding normalized RMS error of 2.3 percent. The normalized RMS error is

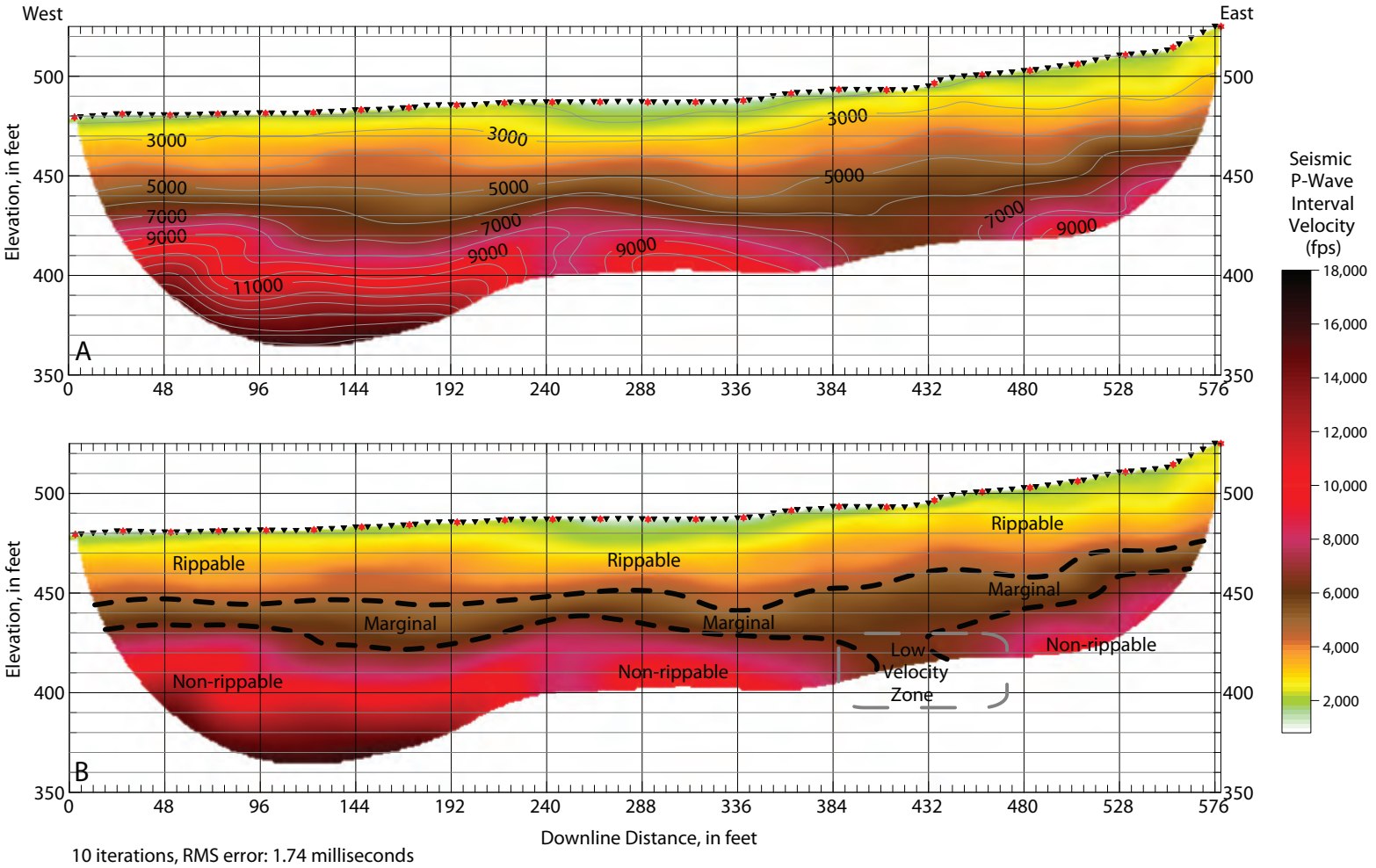

Figure 5. Line A seismic compressional (P-) wave refraction inversion model results. *A*, P-wave velocity profile versus lateral and vertical position, and *B*, an interpretation of general material types is overlaid on the velocity model. The inverted black triangles and red stars along the top of the profiles indicate the geophone and source locations, respectively. The unconsolidated and semi-consolidated materials may be either weathered granodiorite or compacted marine deposits, because they may exhibit the same velocity. The hard rock is material with velocity faster than generally found for even compacted sediment deposits, and is most likely granodiorite. The cause of the low velocity zone at depth is unclear without additional information. (fps, feet per second; RMS, root mean square)

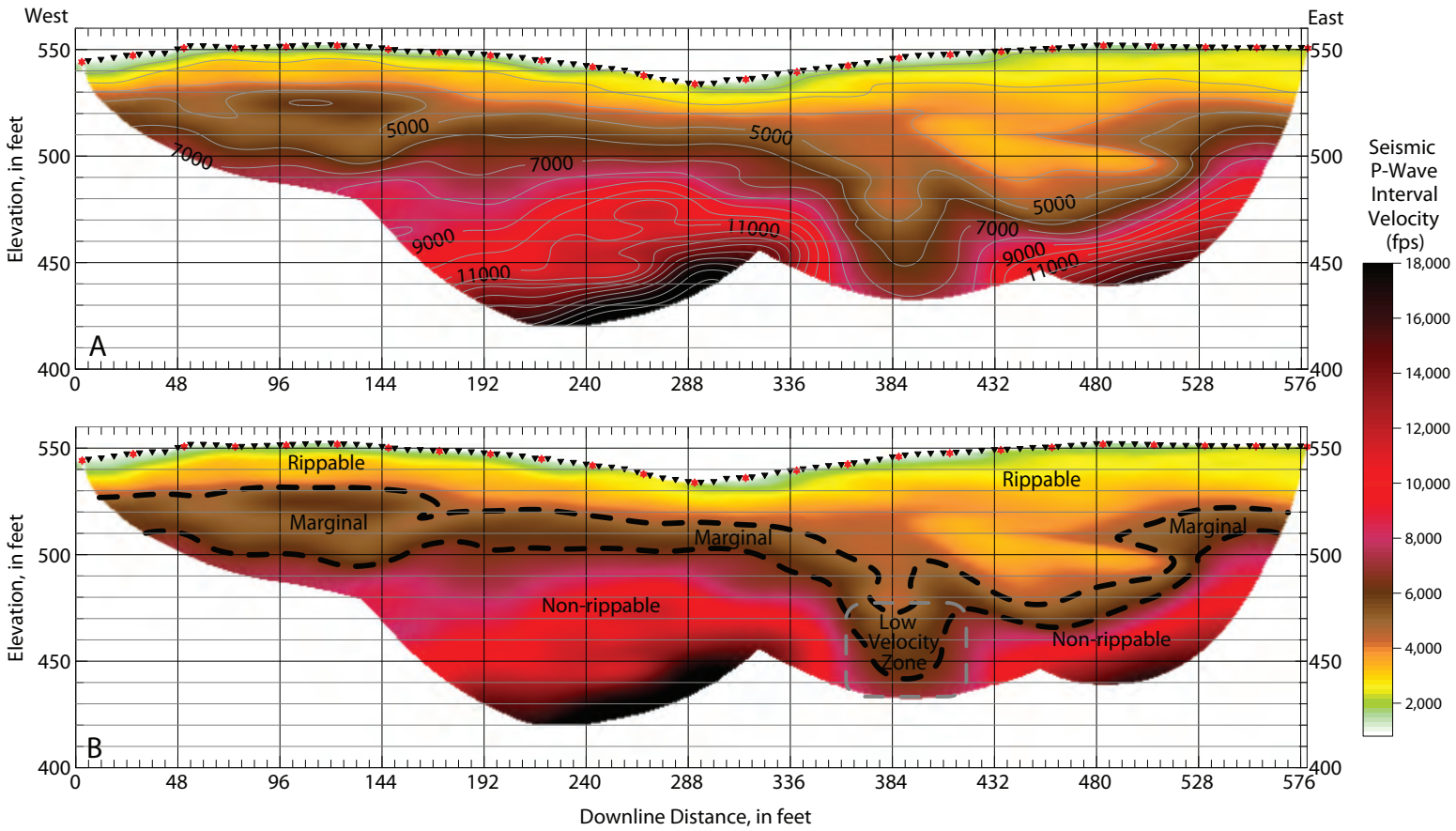

10 iterations; RMS error: 1.34 milliseconds

Figure 6. Line B seismic compressional (P-) wave refraction inversion model results. *A*, P-wave velocity profile versus lateral and vertical position, and *B*, an interpretation of general material types is overlaid on the velocity model. The inverted black triangles and red stars along the top of the profiles indicate the geophone and source locations, respectively. The shallowest depth to a more competent bedrock across the site is at about 288 feet downline distance on this profile and is near 50 feet deep. The cause of the low velocity zone at depth is unclear without additional information. (fps, feet per second; RMS, root mean square)

calculated by dividing the RMS error by the maximum first-arrival traveltime of all the traces modeled (1,624 traces for Line A and 1,112 traces for Line B). The RMS error for the tenth-iteration model presented for Line B is 1.34 ms and 2.3 percent.

Figure 5A shows the inversion model of Line A with the lateral and vertical variations in interval velocity displayed. The color velocity image without contours is also presented overlaid with a general interpretation of rippability (fig. 5B) based on an industry-standard chart (Caterpillar Inc., 2010). Figure 6 shows the same images and interpretations for Line B.

The rippability chart (fig. 7) is based on the ability of Caterpillar's smallest ripper, the D8R/D8T, to successfully excavate a material based on its seismic compressional velocity—this is therefore a conservative rippability classification. The chart shows the upper bounds of the rippable and marginal velocity ranges to be about 6,000 and 8,000 feet per second (fps), respectively. The upper bounds on the velocity images are shown at 4,800 and 6,400 fps, respectively, providing for a very conservative possibility of up to 20-percent error in the accuracy of the velocity determinations with depth. Geophysicists traditionally accept a 10-percent error possibility as a rule of thumb, and the true amount of error will depend on all of the unique aspects of the survey. Lateral variabilities in the maximum depth of investigation of the velocity models are due to end-of-line effects and variations in the maximum source-to-receiver offset traveltime data, mostly caused by low signal-to-noise quality in the shot records at the far offsets. Most importantly for this survey, rippable material extends from the surface to a minimum of 18–20 ft depth, which occurs on Line B up at the fence line in the valley. On Line A, along the pedestrian pathway, the depth of rippable material is greater than 30 ft across the entire profile.

Both lines show a significant thickness of marginal zone material and do not show a clear and distinct interface from rippable to non-rippable material. Geologically, this suggests a thick weathered rock zone. However, it is impossible from these data to determine if the geology consists of either (1) thin soil above 50 ft or more of transition from highly weathered to competent rock or (2) an interval of semi-consolidated marine terrace material below the soil, but above a thinner transition from weathered to competent rock. This is because weathered bedrock and semi-consolidated marine terrace deposits may have similar velocity.

There is a low-velocity zone that is present on both profiles at depth between 385 and 470 ft downline distance on Line A (fig. 5) and between 375 and 415 ft downline distance on Line B (fig. 6). Without additional data or information about the subsurface in this area, it is not possible to determine the cause of this low-velocity zone. This could be a buried erosional feature on the bedrock (such as a valley that becomes broader moving downslope), or the bedrock surface in this area may simply undulate and therefore extend to a depth beyond the maximum depth of investigation. The lower velocity may also be indicative of a more highly fractured or faulted section of bedrock. Faults have been identified on the Monterey peninsula, but none have been previously identified directly through this site. The locations of the low-velocity zones on both profiles suggest a feature that trends approximately north-northwest across the site (fig. 2). Several previously identified Quaternary faults exist less than 15 ka to the southeast of the survey site: the Sylvan thrust and Hatton Canyon faults of the Monterey Bay-Tularcitos fault zone, Seaside-Monterey section (fig. 8; U.S. Geological Survey, 2011). No evidence to date has shown that the Quaternary faults extend through this area.

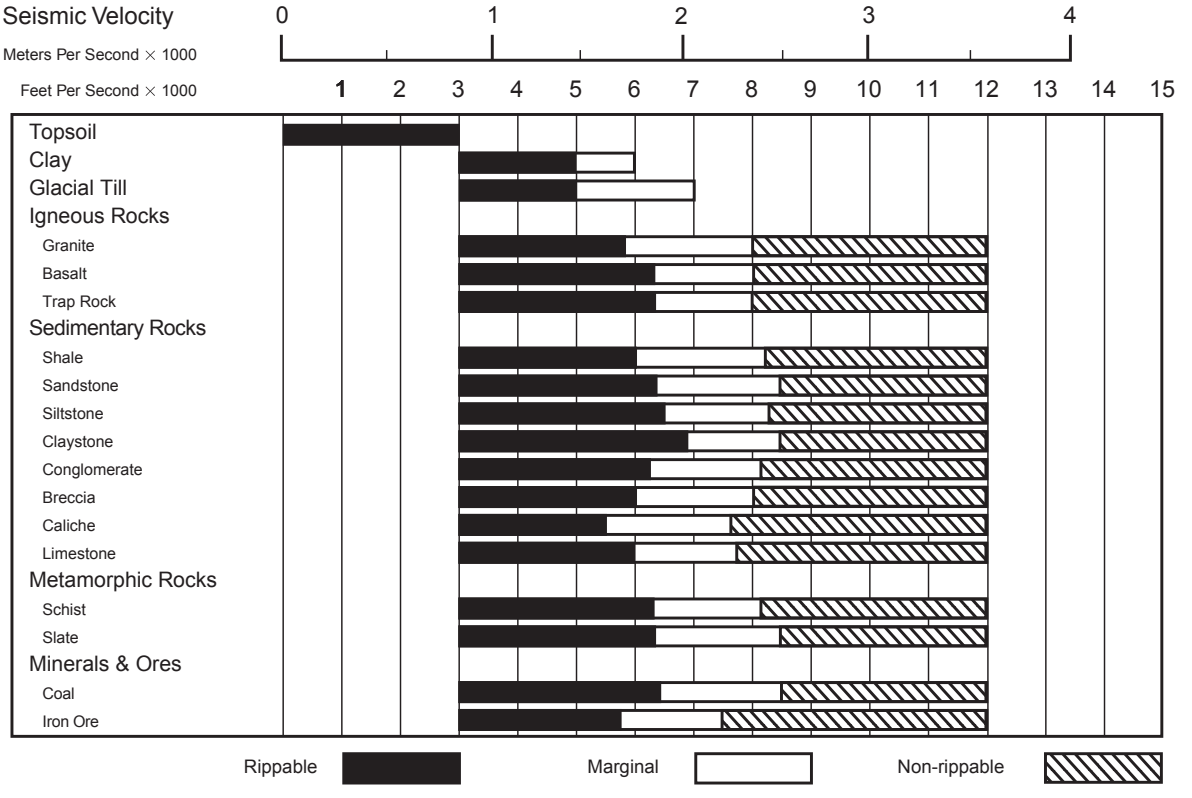

Figure 7. Rippability chart displaying the correlation between seismic compressional-wave velocities, lithologic types, and rippability classification (Caterpillar Inc., 2010). This chart is for the Caterpillar D8R/D8T ripper performance, the smallest Caterpillar excavator available.

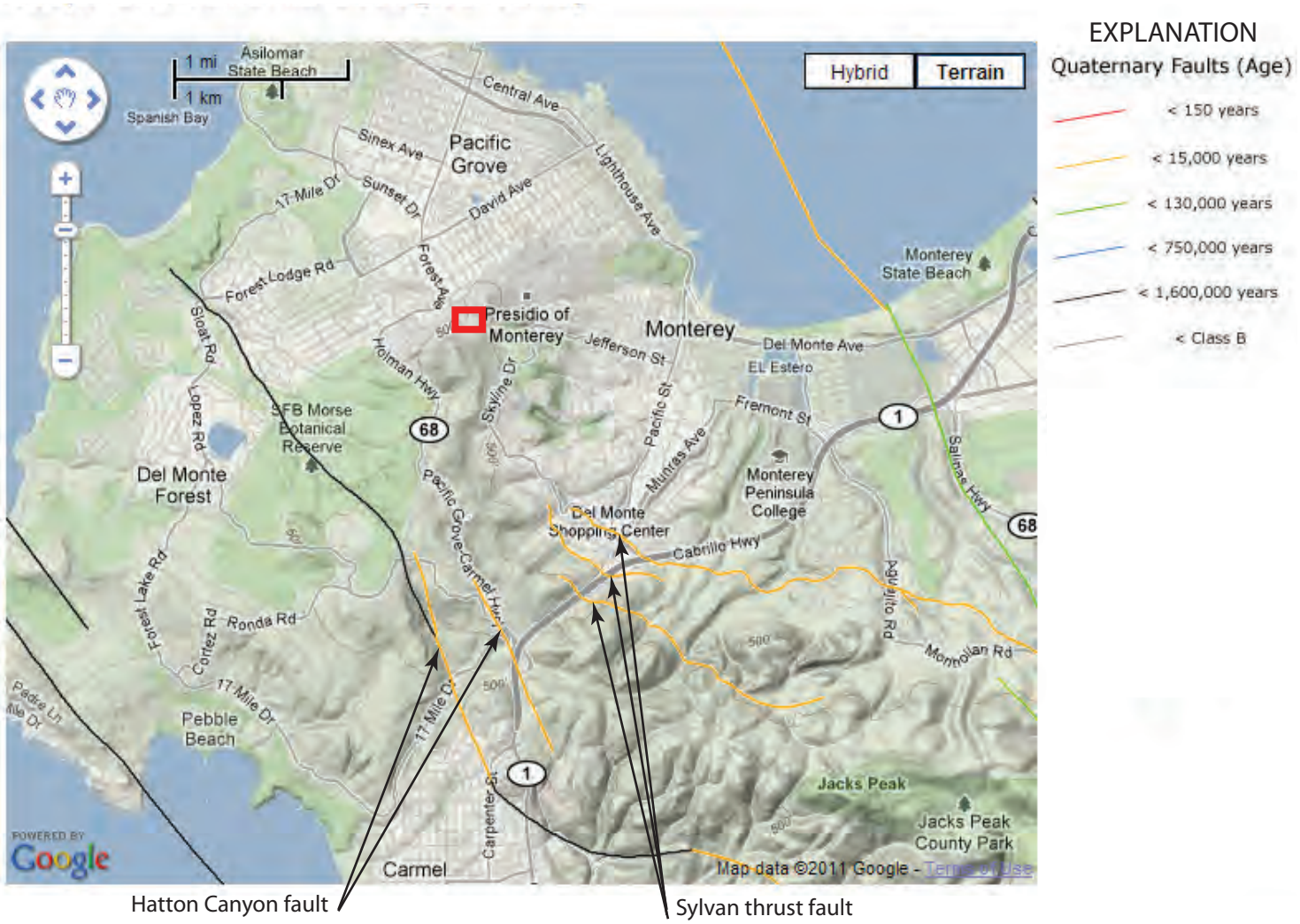

Figure 8. Terrain map showing the locations of previously mapped Quaternary faults on the Monterey peninsula (U.S. Geological Survey, 2011) in the area surrounding the seismic survey site. The seismic survey site is indicated by the red rectangle. Contour interval is 100 feet.

Additional data from trenching, boreholes, LiDAR, or geophysics are necessary to better understand this low-velocity zone.

Conclusions

The seismic refraction tomography models along two sub-parallel profiles acquired at the Presidio of Monterey site indicate that rippable material extends to at least 30 ft depth under the pedestrian pathway corridor (Line A), and to a minimum of 18–20 ft depth under the fence line (Line B). The models show a transition to increasingly more consolidated material with depth. Non-rippable rock is present at depth across the profiles except within a narrow zone just east of the center of Line B and across a broader zone on the east side of Line A.

Acknowledgments

The authors acknowledge and appreciate the field assistance of John Jackson of the U.S. Army Corps of Engineers, Sacramento District, and of Christine Houts, USGS volunteer. Lorrie Madison, biologist, and Will Meyer, Presidio of Monterey project manager, provided much-appreciated help with field logistics. We acknowledge and thank Curtis Payton, Lewis Hunter, and Randy Born at the U.S Army Corps of Engineers, Sacramento District, for their help in making this survey possible.

References Cited

Bailey, A.D., 1975, Rock types and seismic velocity versus rippability, *in* Proceedings of the 26th Annual Highway Geology Symposium, Coeur d'Alene, Idaho, August 13–15, 1975, p. 135–142.

Beck, A.E., 1981, Physical principles of exploration methods: New York, Wiley, 234 p.

Caterpillar Inc., 2010, Caterpillar performance handbook (40th ed): Caterpillar, Inc., Peoria, Ill., 1, 442 p.

Clark, J.C., Dupre, W.R., and Rosenberg, L.I., 1997, Geologic map of the Monterey and Seaside 7.5-minute quadrangles, Monterey County, California—A digital database: U.S. Geological Survey Open-File Report 97–30.

MacGregor, F., Fell, R., Mostyn, G.R., Hocking, G., and McNally, G., 1994, The estimation of rock rippability: Quarterly Journal of Engineering Geology, v. 27, p. 123–144.

Reynolds, J.M., 1997, An introduction to applied and environmental geophysics: Wiley, NY, 796 p.

Rosenberg, L.I., and Clark, J.C., 1994, Quaternary faulting of the greater Monterey area, California: Technical report to U.S. Geological Survey, under Contract 1434-94-G-2443, 27 p., scale 1:24,000.

Schuster, G.T., and Quintus-Bosz, A., 1993, Wavepath eikonal traveltime inversion—Theory: Geophysics, v. 58, p. 1314–1323.

Sharma, P.V., 1997, Environmental and engineering geophysics: Cambridge, United Kingdom, Cambridge University Press, 475 p.

U.S. Geological Survey, 2011, California quaternary faults: U.S. Geological Survey, Geologic Hazards Science Center, accessed online November 2011, at http://geohazards.usgs.gov/qfaults/ca/California.php.

Appendix 1: Seismic Refraction Traveltime Curves

For all seismic data acquired on lines A and B, the refraction tomography P-wave velocity models are created from first-arrival traveltime picks made for every shot record. The picks are displayed as traveltime curves. The downline distance at which each curve converges to zero time represents the shot location. The slope of the curve represents apparent velocity of the energy arrival. Depth to a higher-velocity layer is related to the time at which the curves show a change in slope.

In this appendix, all picked traveltime curves are shown for both lines. The horizontal axis in the plots represents downline distance, in feet. Geophone spacing is 6 ft for both lines, with the first geophone at 6 ft downline distance. The curves are plotted from west to east.

Accurate picks from clean data show a degree of “parallelism” with adjacent closely-spaced curves changing only slightly. Large changes in the shape of an individual curve unrelated to the trend of adjacent curves generally indicate noisy data and less accurate traveltime picks.

The black, dashed lines are sections where first-arrival traveltimes were not picked. For an individual shot, the curve also does not extend across the entire spread because of a low signal-to-noise ratio that prevented clear picks of traveltimes at far offsets. The curves are variously colored for display purposes only that do not have a particular significance.

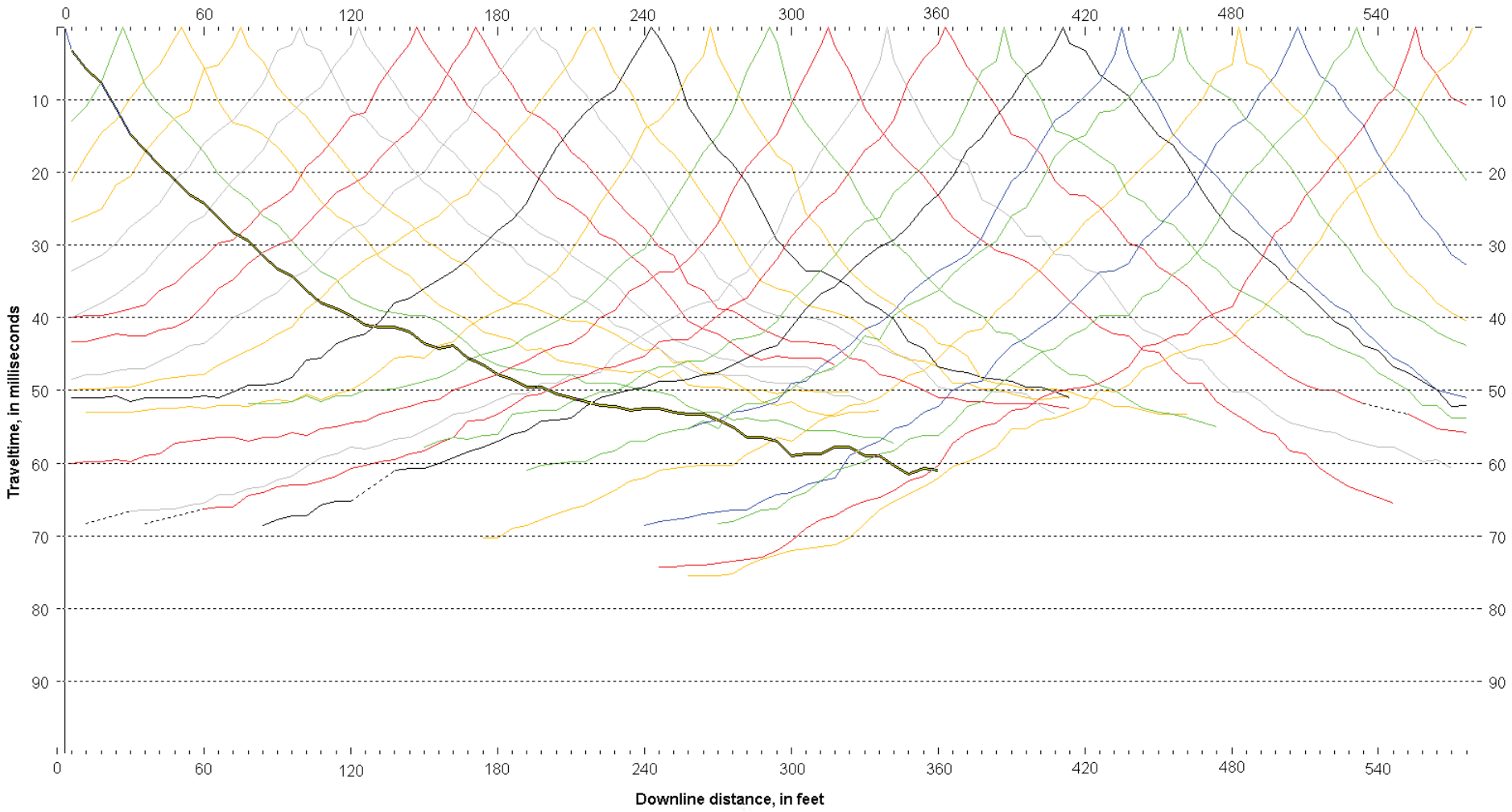

Figure A1. First-arrival traveltime curves for Line A.

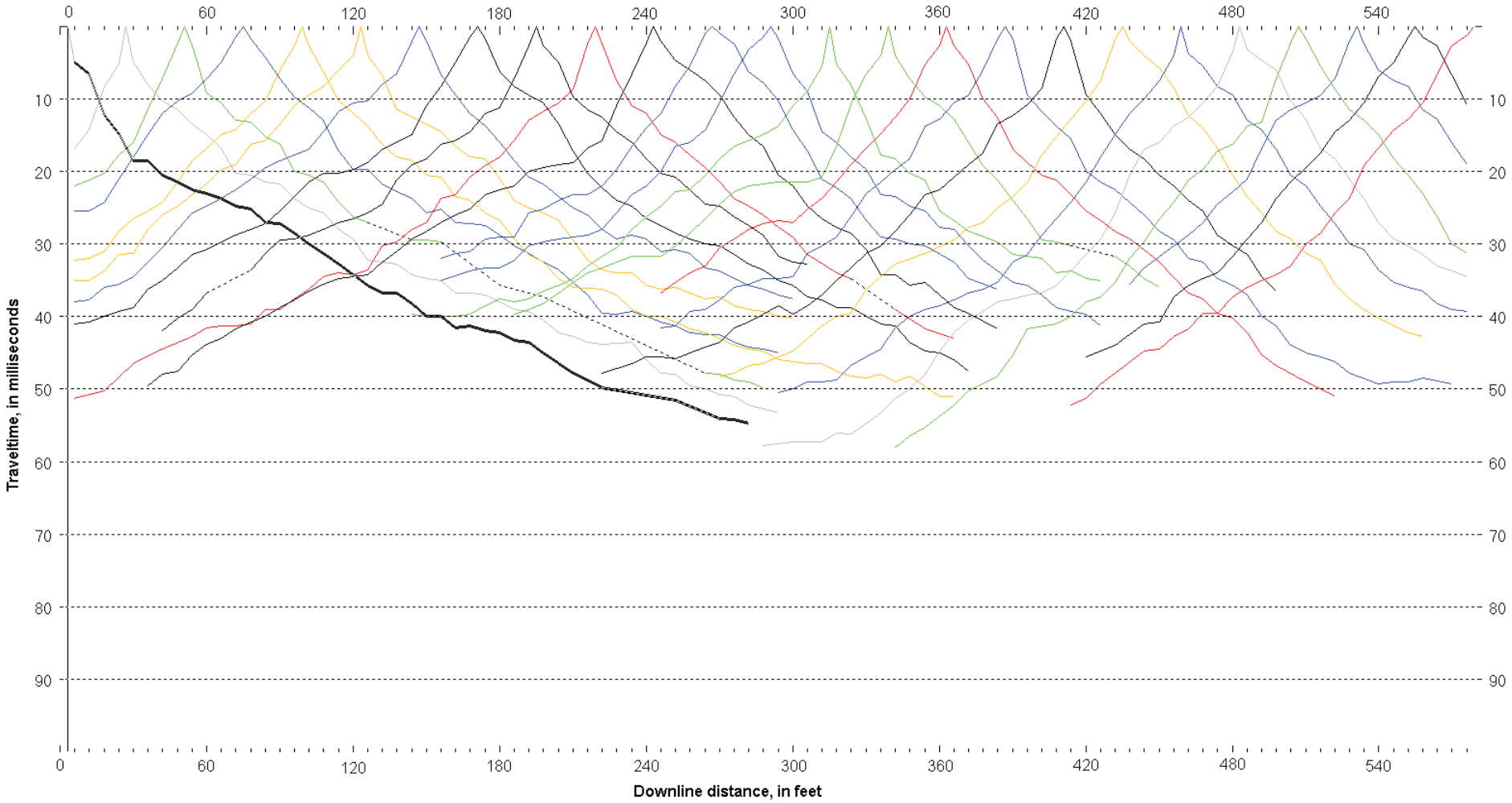

Figure A2. First-arrival traveltime curves for Line B.